Journal Pre-proofs

Bioinspired multiscale hierarchical structure enables solar-thermal conversion for low-temperature aqueous electrochromic device

Qi Zhao, Xue Chen, Qiming Zhu, Chin Ho Kirk, Jianguo Sun, Li Wang, Shuai Guo, Swee Ching Tan, Yanfeng Gao, John Wang

PII: S1385-8947(24)05224-0
DOI: https://doi.org/10.1016/j.cej.2024.153735
Reference: CEJ 153735

To appear in: *Chemical Engineering Journal*

Received Date: 6 May 2024
Revised Date: 19 June 2024
Accepted Date: 3 July 2024

Please cite this article as: Q. Zhao, X. Chen, Q. Zhu, C. Ho Kirk, J. Sun, L. Wang, S. Guo, S. Ching Tan, Y. Gao, J. Wang, Bioinspired multiscale hierarchical structure enables solar-thermal conversion for low-temperature aqueous electrochromic device, *Chemical Engineering Journal* (2024), doi: https://doi.org/10.1016/j.cej.2024.153735

Bioinspired Multiscale Hierarchical Structure Enables Solar-thermal Conversion for Low-temperature Aqueous Electrochromic Device

Qi Zhao,[1] Xue Chen,[3] Qiming Zhu,[5,6]* Chin Ho KIRK,[1] Jianguo Sun,[1] Li Wang,[3] Shuai Guo,[1] Swee Ching Tan,[1] Yanfeng Gao,[3,4]* John Wang[1,2]*

[1]Department of Materials Science and Engineering, National University of Singapore, Singapore, Singapore

[2]National University of Singapore (Chongqing) Research Institute, Chongqing Liang Jiang New Area, Chongqing, China, 401120

[3]School of Materials Science and Engineering, Shanghai University, Shanghai, P. R. China

[4]School of Chemical and Environmental Engineering, Anhui Polytechnic University, Wuhu, P. R. China

[5]Key Lab of Structures Dynamic Behavior and Control of the Ministry of Education, Harbin Institute of Technology, Harbin, People's Republic of China

[6]Key Lab of Smart Prevention and Mitigation of Civil Engineering Disasters of the Ministry of Industry and Information Technology, Harbin Institute of Technology, Harbin, People's Republic of China

*Corresponding author. Email: Dr. Qiming Zhu: zhu_qiming@hit.edu.cn; Prof. Yanfeng Gao: yfgao@shu.edu.cn; Prof. John Wang: msewangj@nus.edu.sg

Abstract

Solar-thermal conversion can mitigate the inadequate electrochemical performance in extreme cold environment for aqueous electrochromic devices (AEDs). However, the limited intrinsic absorptance of electrochromic materials impedes a satisfying solar-thermal conversion. Herein, bioinspired by the *Paradisaeidae*'s super black feathers, multiscale hierarchical structure is purposely made to compose of WO_{3-x} nanowires (WNWs) and silver nanowires (AgNWs), where WNWs are grown on AgNWs in different orientations (denoted as WAg). Our ray tracing simulation reveals its underlying absorption mechanism, demonstrating both an increased optical path and a concentrated energy distribution. Comparably, the WAg-AED exhibits much enhanced absorption (87.0 *vs.* 68.5 % across the entire solar spectrum) and a broader surface temperature change (51.2 *vs.* 39.7 °C within 8 minutes) under 1 solar illumination. This leads to a rapid recovery of electrochromic/electrochemical performance even conducted at -20 °C. Notably, upon irradiation for 12 minutes, the areal capacities of WAg-AED at 0.5 mA cm^{-2} increase by 3.8 and 1.7 times, when compared to the device operating at -20 °C and room temperature, respectively. The WAg-AED establishes a close connection between the photo-thermal conversion and electrochemistry, proving a new pathway in the development of sustainable electronics.

Keywords Multiscale hierarchical structure, Bioinspired pathway, Aqueous electrochromic device, Solar-thermal conversion

1 Introduction

Owing to the enhanced safety and electrochemical kinetics, aqueous electrochromic devices (AEDs) have been widely studied for integration into internet of things (IoT), wearable electronics, and sensors.[1-3] Nonetheless, AEDs also encounter challenges in association with the sluggish ionic mobility and electrolyte freezing at sub-zero temperatures, as well as reduced overall lifespan.[4-6] Numerous efforts have been made to enhance the environmental endurance for AEDs. Improving the durability of electrolyte is one of a prominent strategy. For example, engineering an eutectic with organics effectively lowers the freezing point of electrolyte.[7] Besides, raising the concentration of inorganic can widen the operating temperature range, known as the "water-in-salt electrolyte".[8,9] However, various kinetic issues in the interior and/or surface of electrodes have not been addressed.[10] Low-temperature conditions impose substantial issues of low kinetics for the chemical reactions, which is typically observed during the charge and discharge even at room temperature, due to insufficient thermal kinetic energy provided by the surrounding environment.[11]

In this context, solar-thermal conversion is proposed as a cost-effective thermal management to maintain the temperature in a rational range.[12,13] Initially, this concept is applied to elevate the surface temperature of supercapacitors, with typical electrode materials such as graphene,[14] Ni/Co-layered double hydroxide,[15] and spinel-type $Cu_{1.5}Mn_{1.5}O_4$, [16]. It is noteworthy that these materials possess exceptional absorption (>90 %) over the entire solar spectrum but lack electrochromic effects. To the best of our knowledge, this thermal management strategy has not been reported in AEDs. Only one pioneering study has utilized the electrochromic effect of PBA/NiO as the electrode to enhance the local surface temperature of supercapacitors. However, it achieves only an undesired accelerated temperature rise (>30 min) due to the low absorption across the entire solar spectrum (<60 %).[17] According to the Beer-Lambert law ($I(x) = I_0 e^{-\alpha x}$),[18,19] the light energy $I(x)$ decades exponentially during the refraction process, where x is the optical path length, α is the absorption coefficient. Hence, developing an ideal structure to extend the optical path length emerges as an effective strategy to enhance solar-thermal conversion.

Through millions of years of natural selection, one species of birds of paradise (Aves: *Paradisaeidae*) have developed strikingly black plumage patches that are significantly darker than usual black plumage observed in closely related species (**Fig. 1a-1b**).[20] This structural absorption of "super black" is achieved by hierarchical structures featuring microscale spikes along the margins. The barbule arrays in feathers exhibit dimensions with 200-400 μm depth and 5-30 μm width, whereas the cavities along the barbule margins are on a smaller scale of less than 5 μm (**Fig. 1c-1d**). As a result, this multi-scale hierarchical structure renders multi-reflection of light and increases optical path.[21-24] A similar mechanism has also been observed in both black snake scales and butterfly scales to keep their body warm in cold weathers.[25-28]

Herein, solar-thermal conversion is proposed to address the undesirable electrochromic performance in extreme-cold environments through enhancing multi-reflection and extending optical path (**Fig. 1e**). A bio-inspired multi-scale hierarchical structure (denoted as WAg, **Fig. 1f**) is purposely designed, comprising WO_{3-x} nanowires (WNWs) with a mean diameter of 3-5 nm and length of 50-70 nm), and silver nanowires (AgNWs) with a mean diameter of 30-70 nm and length of 30-40 um. Incident light enters *via* either Path 1 or Path 2 (**Fig. S1**), multiple reflections occur at the surface either AgNWs or WNWs, as if light becomes trapped in this structure.[21] Our AED features a multilayer configuration consisting of ITO-PET/WAg/$ZnCl_2$/Zn/ITO-PET, with WAg serving as the cathode (**Fig. 1g**). Consequently, this structure enables WAg-AED to rapidly recover to its initial performance at room temperature within 8 minutes even at -20 °C. Additionally, in contrast to those mainstream energy storage devices characterized by constant absorption, such as batteries and supercapacitors, we envision that AEDs can also mitigate the safety risks and uncomfortable wearability associated with abundant sunlight, owing to their tunable absorption capability. By establishing a direct relationship between the photo-thermal conversion and electrochemistry, we aim to expand the applications of AED in a sustainable manner.

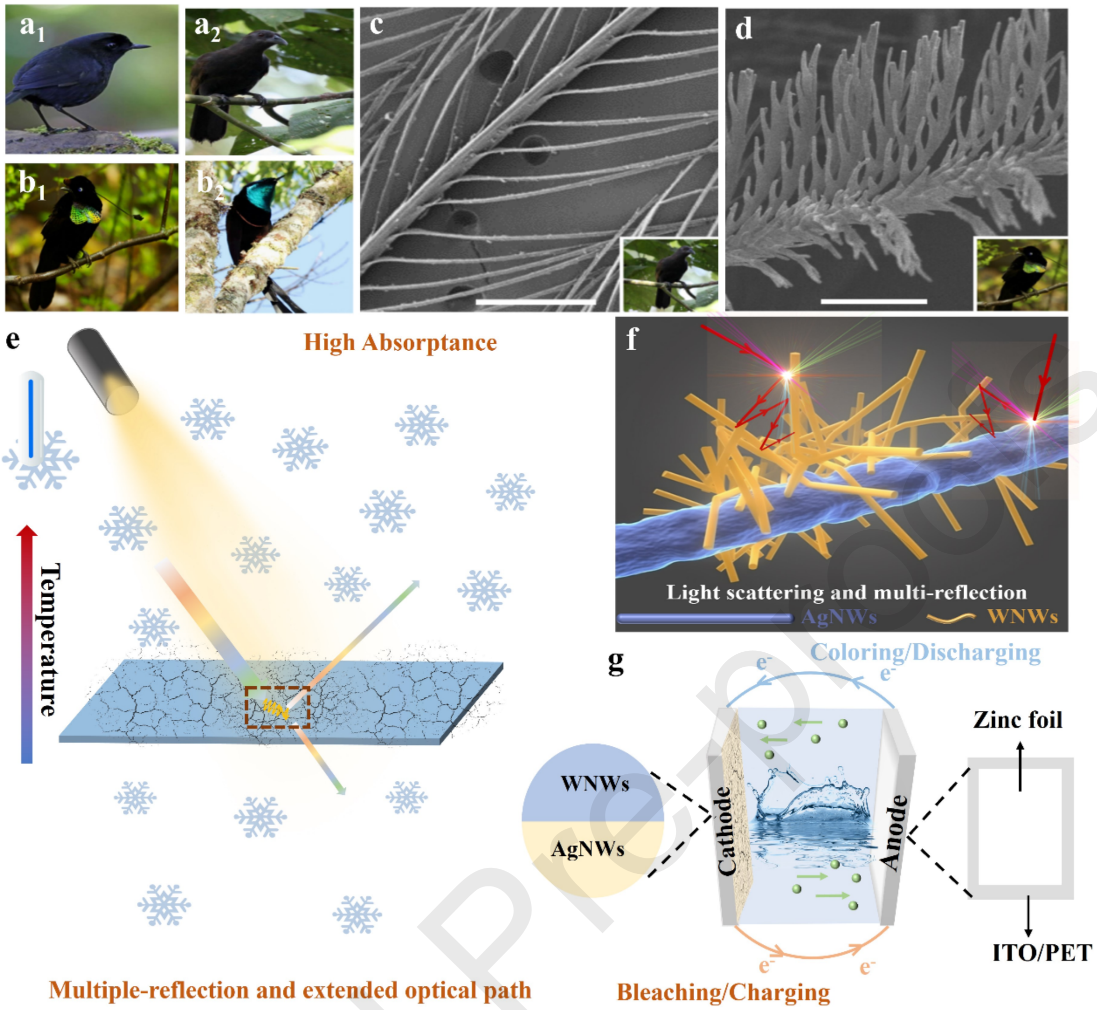

Fig. 1 Examples of birds with normal and super-black feathers in nature (a-d), along with the concept of bioinspired multiscale hierarchical structures for solar-thermal conversion (e-g). Digital photographs of *Melampitta lugubris* (a_1) *and Lycocorax pyrrhopterus* (a_2) with normal black feathers, and *Parotia wahnesi* (b_1) and *Astrapia stephaniae* (b_2) with super black feathers. Corresponding SEM images of normal black feathers (c) and super black feathers (d). Reproduced with permission.[20] Copyright 2018, Springer Nature. (e) Schematic illustration of concept of solar-thermal conversion at low temperature. (f) Schematic illustration of WAg electrode with strong light scattering and multi-reflection. (g) Device configuration of WAg-AED.

2 Results and Discussion

2.1 Simulation on Structural Absorption Mechanism

The structural absorption mechanism of WAg is simulated by ray tracing techniques.[29,30] AgNW and WNW are represented as cylindrical structures, while the incident light is treated as parallel rays. Comprehensive information regarding the modeling details can be found in the supplementary material (Section 1.8). The optical paths at visible wavelength (700 nm) and near-infrared wavelength (1500 nm) for WAg are simulated in **Fig. 2**. The average energy absorption rates at 700 nm and 1500 nm with AgNWs are 6.3 % and 5.6 % higher, respectively, compared to those without AgNWs (**Fig. 2a-2b** and **Fig. S2a-S2b**). The improvement is attributed to the greater number of light intersections in WAg, as well as the longer optical path (**Fig. 2c-2d** and **Fig. S2c-S2d**). Typically, the diameter of AgNWs is significantly larger than that of WNW, which increases the packing ratio of WAg and enhances the light-matter interactions between a single ray and the object. Furthermore, the highly reflective nature of AgNWs results in at least 90 % reflection of incident light. AgNWs are situated beneath the WNWs, thereby mitigating initial light reflection. This arrangement increases the likelihood of ray-WNW intersections, thereby significantly extending the optical path. The corresponding energy distributions for WAg and WNW conducted at 700 nm and 1500 nm provide more evidence (**Fig. 2e-2f** and **Fig. S2e-S2f)**. The color point represents the absorption location where the incident light occurs, while the depth of color indicates the intensity of absorption. The heat distributions in the colored WAg are more intense than those in the colored WNWs, especially around the interface between AgNWs and WNW. Therefore, our WAg effectively "traps" the light and energy within its internal structure, further enhancing the solar-thermal conversion.

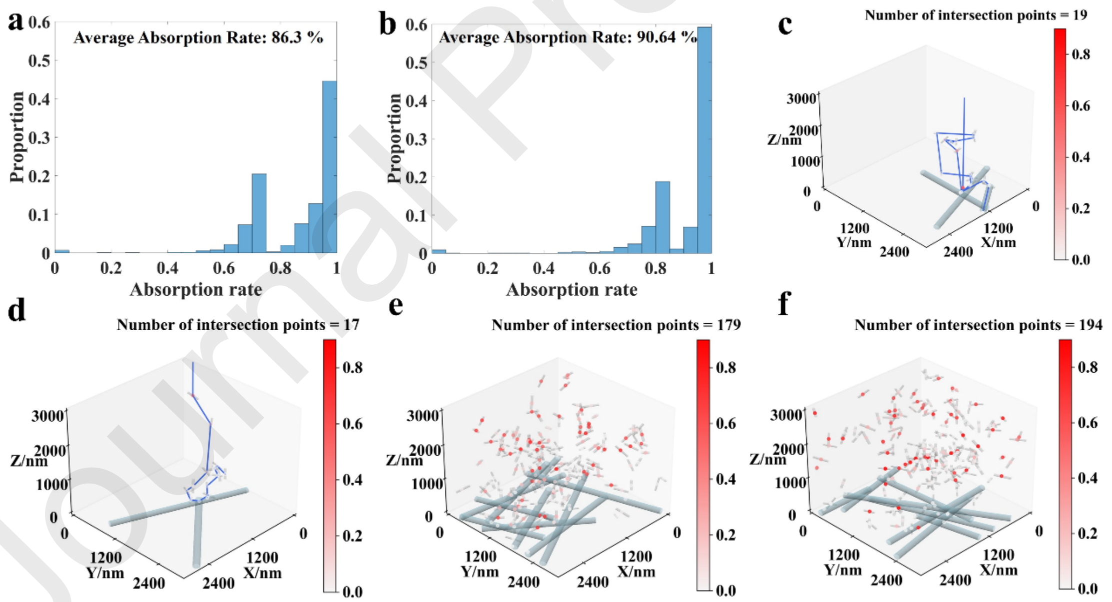

Fig. 2 Ray tracing simulation of absorption mechanism of WAg-AED conducted at 700 and 1500 nm. Histogram of absorption rates of each light path for the colored WAg-AED conducted (a) at 700 nm and (b) at 1500 nm. Simulated optical path of the colored WAg-AED conducted (c) at 700 nm and (d) at 1500 nm. Simulated heat distribution of the colored WAg-AED conducted (e) at 700 nm and (f) at 1500 nm. The color bar value corresponds to the relative ratio of ray absorption, indicating the proportion of current ray energy to the initial ray energy. A value of 1.0 signifies complete absorption of all energy.

2.2 Demonstration of Solar-thermal Conversion of WAg-AED

The specific phase and morphology characterizations of WAg are presented in **Fig. S3-S5**. WNWs and AgNWs are synthesized using our previous methods.[1,31,32] Typically, WAg structure, with WNWs (with a mean diameter of 3-5 nm and length of 50-70 nm) randomly attached to AgNWs (with a mean diameter of 30-70 nm and length of 30-40 um) in different orientations, is illustrated in **Fig. 3a-3c** and **Fig. S5**. The significant size differences and the arrangements of AgNWs and WNWs induce robust light scattering and extend the length of light-matter interaction, thereby significantly enhancing the collection of incident light and raise the temperature.[33-36] **Fig. 3d** shows the thickness of each layer, including the WNW layer, the AgNWs layer and ITO conductive layer.

Experimentally, *in-situ* absorptance spectra of the WAg and WNWs electrode in colored states are shown in **Fig. 3e**. The colored WAg demonstrates an absorption of 87.0 % ranging from 2500 nm to 380 nm (**Equation S1** in supporting information), surpassing the absorption of the colored WNWs (68.5 %), and achieving comparable absorption of typical supercapacitor electrode materials (55.2 %-91.7 %, **Table S1**). This enhancement is consistent with our ray tracing simulations.

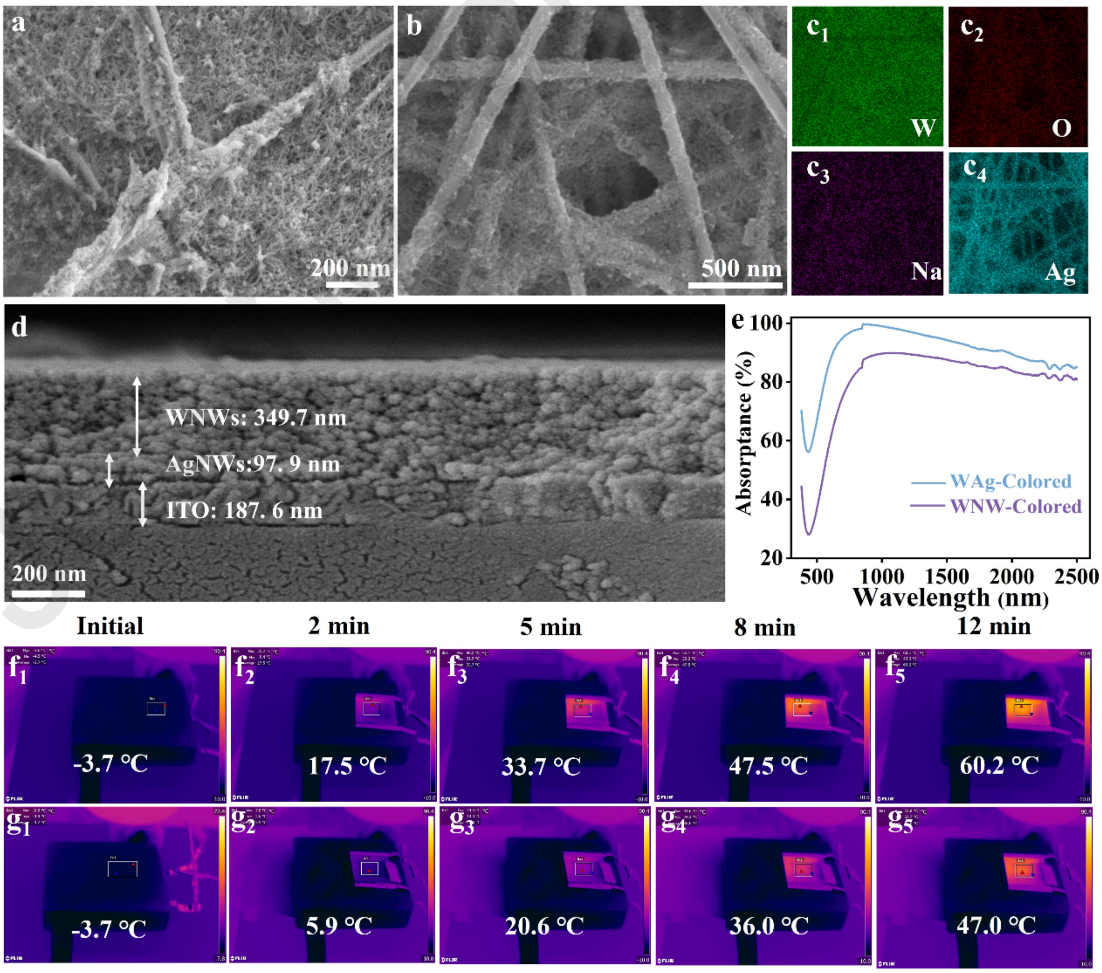

Fig. 3 Demonstration of solar thermal conversion for AED at low temperature. (a-b) SEM images of the WAg electrode with multiscale hierarchical structure. (c) the corresponding EDS results. (d) Cross-section SEM image of the WAg film. (e) The entire-solar-spectrum absorptance of the WAg and the WNWs. (f) Infrared images of WAg-AED and (g) WNW-AED conducted at -20 °C with different irradiation time.

To evaluate the photo-thermal capability of WAg-AED for potential practical applications, the demonstrations are conducted utilizing solar light. An integrated testing system is custom-built (**Fig. S6**). The test is conducted at -20 °C under 1 solar illumination. As a result, the surface temperature swiftly recovers from -3.7 °C to 33.7 °C within only 5 mins (**Fig. 3f**), while the WNW-AED exhibits a lower temperature of 20.6 °C (**Fig. 3g**). With the irradiation time increasing to 8 mins, the surface temperature of WAg-AED reaches 47.5 °C, surpassing both WNW-AED (36.0 °C) and the temperature reported in the NiO/PB work(<30 °C).[17] The relationships between the surface temperature and irradiation time are summarized in **Fig. 4a**. The rate of temperature increase in WAg-AED is consistently higher than that in WNW-AED, indicating that the WAg structure possesses superior photothermal conversion capabilities.

A comprehensive analysis of the relationship between the electrochromic/electrochemical performances of the WAg-AED and the irradiation time is conducted at -20 °C. The applied potential window ranges from +0.2 V to +1.2 V, with an interval time of 20 s. As shown in **Fig. 4b**, the device experiences a significant deterioration at -20 °C in optical contrast (27.6 % vs. 55.2 %) and switching speed (10/13.5 s vs. 4.5/6.5 s), as compared to its performance at room temperature. The specific performance indicators are summarized in **Table S2**. To better understand the recover capability under solar irradiation, we normalize the optical contrast and switching speed, where the green dotted line represents the performance of AED conducted at room temperature (**Fig. 4c and 4d**). With prolonged irradiation, electrochromic performances gradually restore to their initial states. Notably, WAg-AED fully restores its original optical contrast and switching speed after an 8-min irradiation period, whereas WNW-AED fails to achieve such restoration even after 12 mins of irradiation (**Fig. S7** and **Table S3**). Similar results are observed in coloration efficiency (**Fig. 4e** and **Fig. S8**). The values are calculated using **Equation S2** in supporting information. As the irradiation time increases, the coloration efficiencies of WAg-AED rise from 32.0 to 98.7 cm^2C^{-1}, eventually surpassing the performance at room temperature (91.4 cm^2C^{-1}). **Fig. 4f** shows that the recovery speed of WAg-AED is more rapid than that of WNW-AED, suggesting the better solar-thermal conversion. Interestingly, while the devices show stable cycling performance at room temperature, they fail to operate at -20 °C after 100 cycles (**Fig. S9-S10**). However, upon irradiation, they can endure more than 100 cycles (**Fig. 4g**). Notably, as the irradiation time extends to 12 minutes, the electrochromic performance of our AED surpasses that achieved under room temperature conditions (**Table S2-S3**). This achievement also demonstrates a competitive advantage over previously reported AEDs (**Table S4**).[37-43] Furthermore, a common observation for the device in low temperature environments is the occurrence of uneven color changes, accompanied by the emergence of a foggy phenomenon on the device surface (**Fig. S11a-S11b**). However, the WAg-AED device, even in large-size configuration (10 cm × 15 cm), exhibits a stable switching process facilitated by solar irradiation (**Fig. S11c-S11d**).

In addition, galvanostatic charge-discharge (GCD) curves performed with irradiation time are presented in **Fig. 4h**. WAg-AED exhibits poor areal capacity of 36.7 mAh m^{-2} at the current density of 0.5 mA cm^{-2} in cold environments, while the capacity gradually restores to initial state under solar irradiation. The normalized capacity is shown in **Fig. 4i**. As the irradiation time exceeds 8 minutes, the capacities of WAg-AED surpass those achieved at room temperature. Within a 12-minute irradiation period, the capacity of the WAg-AED increases by 1.7 and 3.8 times, compared to the initial performance conducted at room temperature and -20 °C, respectively (139.3 *vs.* 82.7 *vs.* 36.7 mAh m^{-2}). Significantly, WAg-AED also exhibits an outstanding areal capacity after irradiation in the electrochromic device/battery with an identical configuration (77.1 mAh m^{-2} at 0.2 A m^{-2},[44] 101.1 mAh m^{-2} at 0.25 mA cm^{-2},[9] 106.7 mAh m^{-2} at 0.25 mA cm^{-2},[45] 126.3 mAh m^{-2} at 0.25 mA cm^{-2},[2] 127.8 mAh m^{-2} at 0.06 mA cm^{-2} [46]). This significant improvement effectively solves the dilemma of poor electrochemical performance typically observed in electronics operating at low temperatures. Although similar trends are also observed in WNWs-AED, the overall restoration rate is notably lower than that observed in WAg-AED (**Fig. S12**).

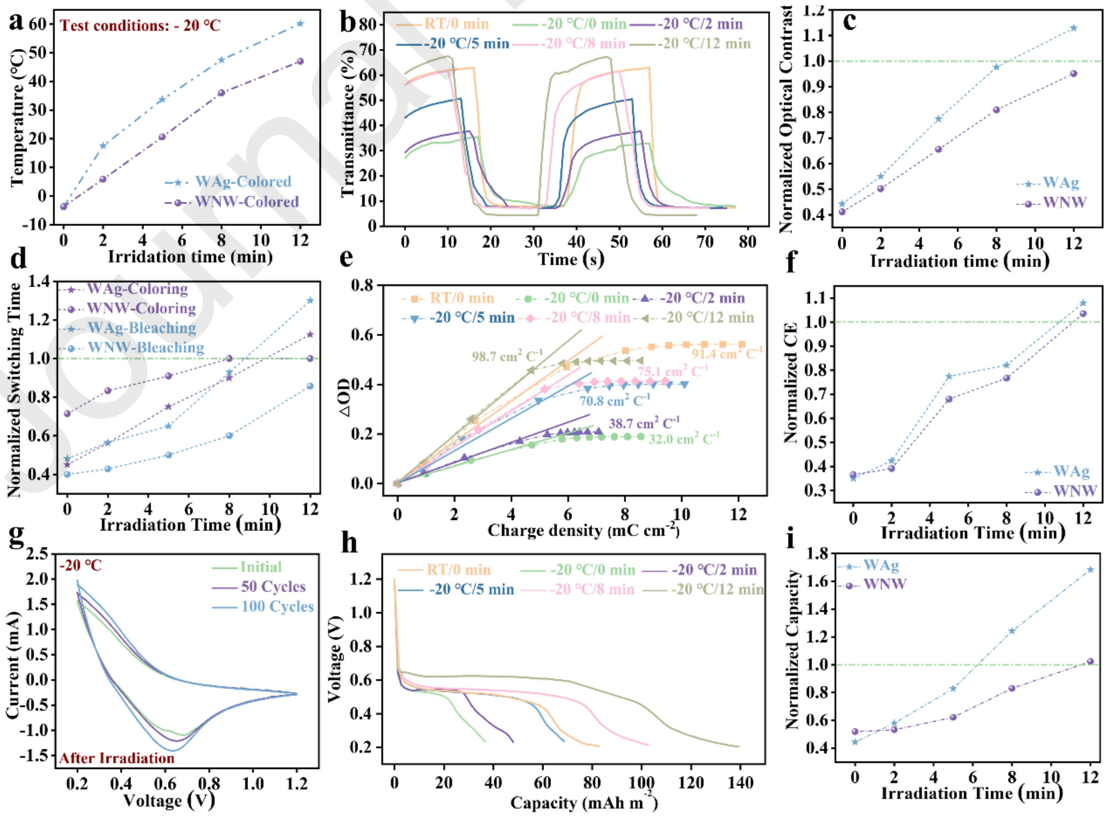

Fig. 4 Electrochromic and electrochemical performances of the WAg-AED conducted at -20 °C under 1 solar illumination irradiation. (a) The relationships between irradiation time and temperature of WAg-AED and WNW-AED conducted at -20 °C. (b) *In-situ* optical modulation (633 nm) of WAg-AED conducted at -20 °C with different irradiation time. (c) Normalized optical contrast of WAg-AED and WNW-AED conducted at -20 °C with different irradiation time. Normalized optical contrast is the ratio of optical contrast under varied irradiation time to optical contrast at room temperature. (d) Normalized switching speed of WAg-AED and WNW-AED conducted at -20 °C with different irradiation time. Normalized switching time is the ratio of switching time at room temperature to switching time under varied irradiation time. (e) Coloration efficiency of WAg-AED conducted at -20 °C with different irradiation time. (f) Normalized coloration efficiency of WAg-AED and WNW-AED conducted at -20 °C with different irradiation time. Normalized coloration efficiency is the ratio of coloration efficiency under varied irradiation time to coloration efficiency at room temperature. (g) Cycling performance of WAg-AED after irradiation. (h) Galvanostatic charge/discharge curves of WAg-AED conducted at -20 °C with different irradiation time. (i) Normalized capacity of WAg-AED and WNW-AED conducted at -20 °C with different irradiation time. Normalized capacity is the ratio of capacity under varied irradiation time to capacity at room temperature.

2.3 Envisioning AEDs and Other Energy Storage Devices for Harsh Environment Applications

In future, we envision a trend towards wearable electronics equipped with self-temperature control, allowing for optimal functionality in extreme temperatures. This involves efficient solar energy absorption in cold environments while preventing device overheating in warmer conditions (**Fig. 5**). The superior photo-thermal conversion capability inherent in mainstream energy storage devices, such as batteries and supercapacitors, is well-suited for cold environments but less applicable in warmer settings. In contrast to those devices with constant absorption, the distinctive advantage of AEDs lies in their tunable absorption capability. For example, transition metal oxide (TMO) materials, such as WO_3, exhibit different corresponding to their varying valence states.[47,48] Comparative analysis of AED and other energy storage devices are discussed in **Fig. S13-S15**. Typically, there is a substantial difference in absorptance of AED between the colored state and the bleached state, decreasing from 87 % to 20.4 % (**Fig. S13** and **Table S5**). **Fig. S14** displays the infrared images of fully bleached of WAg-AED simulated in an outdoor environment with abundant sunlight. Surprisingly, the temperature difference between WAg-AED and supercapacitors can reach 15.1°C, while the temperature difference between WAg-AED and lithium-ion battery can reach 7.8 °C, within only 150 s under 1 solar illumination. The exceedingly low absorption coefficients in the bleached state contribute to a reduced intensity of energy distributions (**Fig. S16** and **S17**). In addition, our AED can function properly under high temperatures (**Fig. S18**). The electrochromic performances of WAg-AED at 40 °C are comparable to those achieved at room temperature, with a slight difference in optical modulation (52.8 % *vs.* 55.2 %). Impressively, the switching speeds exhibit improvements at higher temperatures (t_c: 4 *vs.* 4.5 s, t_b: 5 *vs.* 6.5 s). This trend is also observed with WNW-AED (**Fig. S19** and **Table S6**). This development decreases the safety risks and uncomfortable wearability as well as prevents diminished discharge performance resulting from the high temperatures.

Thus, even in scenarios such as mountain climbing or skiing without direct sunlight at night, the device can effectively recover its energy storage capacity by a simulated light source. On the other hand, in situations with abundant outdoor sunlight, conventional wearable electronics can absorb a significant amount of heat when fully charged, reducing the level of comfort and posing risks of thermal runway. Notably, our WAg-AED with dynamic absorption capability allows for significant reflection of incident light and dissipation of excess heat, mitigating rapid temperature rises.

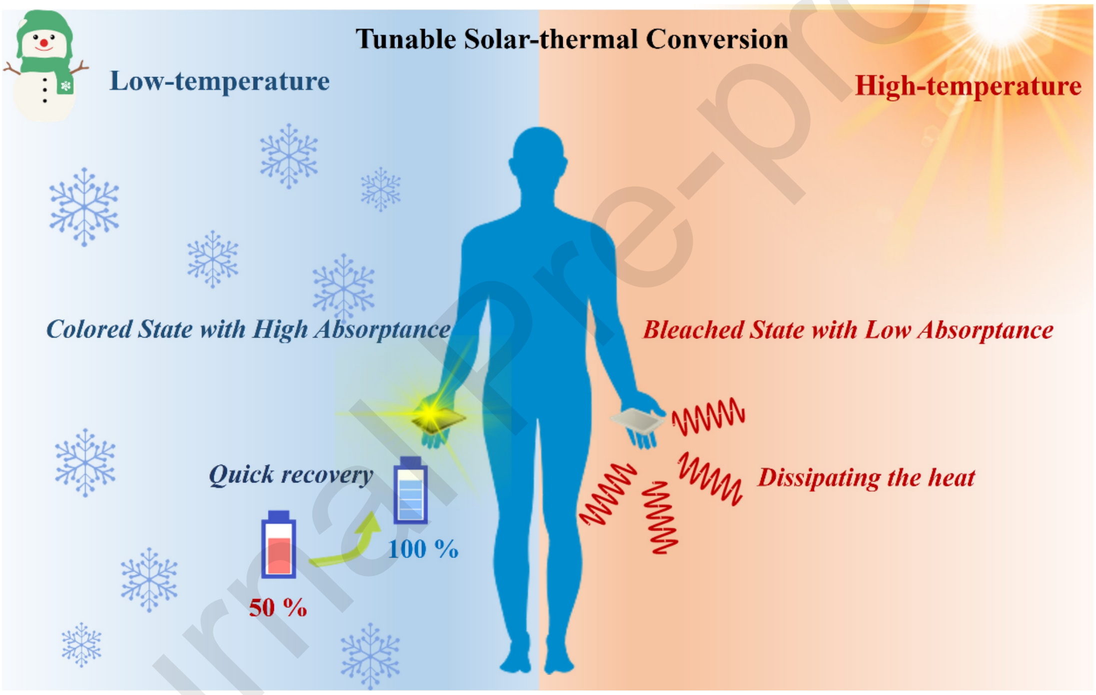

Figure 5. Blueprint of wearable AEDs with self-controlled temperature in harsh conditions. In low temperature, high absorptance and strong photo-thermal conversion capability result in a rapid temperature recovery when exposed to solar illumination. This, in turn, enhances the restoration of electrochromic and electrochemical performance. In high temperature, low absorptance mitigate rapid temperature rises under intense outdoor sunlight, thereby reducing the safety risks and improving wearable comfortability.

3 Conclusion

In summary, bioinspired by the *Paradisaeidae*'s super black feathers, multiscale hierarchical structures consisting of WAg electrode with much enhanced solar-thermal conversion are purposely designed to address the challenges of sluggish kinetics in cold environments. Our ray tracing simulations confirm the absorption mechanism of WAg-AED, revealing the underlying optical pathways and heat distribution. As a result, the designed structures are shown to exhibit the high absorptance of 87.0 % over the whole solar spectrum (ranging from 2500 nm to 380 nm), showing their effectiveness in solving the intrinsic absorption limitations of electrochromic materials. Their electrochemical performance rapidly restores within a brief 8-minute duration, even at -20 °C, under 1 solar illumination. Notably, upon irradiation for 12 mins, the capacities of WAg-AED increase by 3.8 and 1.7 times, compared to the device operated at -20 °C and room temperature, respectively. In addition, compared to the competing energy storge devices (e.g., battery and supercapacitor) with constant absorption, aqueous electrochromic devices with tunable absorption have their potential for applications in wearable electronics, particularly in adapting to extreme cold or heat conditions.

Data availability

All data are shown in the manuscript and/or Supplementary Information. All Python codes employed for ray tracing simulations are accessible upon a written request directed to the corresponding authors.

Author contributions

Q.Z, Y.F.G and J.W conceived the idea of the study. Q.Z performed the synthesis of the materials. Q.Z and X.C characterized the optical, electrochemical and thermal performances. Q.M.Z completed the ray tracing simulation. Q.Z, Q.M.Z, Y.F.G, J.W wrote the paper, and all authors contributed to editing the manuscript.

Acknowledgments

This work is supported by Singapore NRF (NRF-CRP26-2021-0003), research work conducted at the National University of Singapore.

Declaration of interests

The authors declare no competing interests.

References

[1] Q. Zhao, J. Wang, X. Ai, Y. Duan, Z. Pan, S. Xie, J. Wang, Y. Gao, Three-dimensional knotting of $W_{17}O_{47}$@ PEDOT: PSS nanowires enables high-performance flexible cathode for dual-functional electrochromic and electrochemical device, InfoMat 4 (2022) e12298. https://doi.org/10.1002/inf2.12298

[2] H. Li, C.J. Firby, A.Y. Elezzabi, Rechargeable aqueous hybrid Zn^{2+}/Al^{3+} electrochromic batteries, Joule 3 (2019) 2268-2278. https://doi.org/10.1016/j.joule.2019.06.021

[3] Q. Zhao, Y. Fang, K. Qiao, W. Wei, Y. Yao, Y. Gao, Printing of WO_3/ITO nanocomposite electrochromic smart windows, Solar Energy Materials and Solar Cells 194 (2019) 95-102. https://doi.org/10.1016/j.solmat.2019.02.002

[4] D. Chao, W. Zhou, F. Xie, C. Ye, H. Li, M. Jaroniec, S.-Z. Qiao, Roadmap for advanced aqueous batteries: From design of materials to applications, Science advances 6 (2020) eaba4098. https://doi.org/10.1126/sciadv.aba4098

[5] Q. Zhao, Z. Pan, B. Liu, C. Bao, X. Liu, J. Sun, S. Xie, Q. Wang, J. Wang, Y. Gao, Electrochromic-Induced Rechargeable Aqueous Batteries: An Integrated Multifunctional System for Cross-Domain Applications, Nano-Micro Letters 15 (2023) 87. https://doi.org/10.1007/s40820-023-01056-y

[6] Y. Wang, X. Zhong, X. Liu, Z. Lu, Y. Su, M. Wang, X. Diao, A fast self-charging and temperature adaptive electrochromic energy storage device, Journal of Materials Chemistry A 10 (2022) 3944-3952. https://doi.org/10.1039/D1TA10726G

[7] P. Sun, J. Chen, Y. Li, X. Tang, H. Sun, G. Song, X. Mu, T. Zhang, X. Zha, F. Li, Deep eutectic solvent-based gel electrolytes for flexible electrochromic devices with excellent high/low temperature durability, InfoMat 5 (2023) e12363. https://doi.org/10.1002/inf2.12363

[8] Q. Dou, S. Lei, D.-W. Wang, Q. Zhang, D. Xiao, H. Guo, A. Wang, H. Yang, Y. Li, S. Shi, Safe and high-rate supercapacitors based on an “acetonitrile/water in salt” hybrid electrolyte, Energy & Environmental Science 11 (2018) 3212-3219. https://doi.org/10.1039/C8EE01040D

[9] X. Ai, Q. Zhao, Y. Duan, Z. Chen, Z. Zhang, Y. Liu, Y. Gao, Zinc polyacrylamide

hydrogel electrolyte for quasi-solid-state electrochromic devices with low-temperature tolerance, Cell Reports Physical Science 3 (2022) 101148. https://doi.org/10.1016/j.xcrp.2022.101148

[10] N. Zhang, T. Deng, S. Zhang, C. Wang, L. Chen, C. Wang, X. Fan, Critical Review on Low-Temperature Li-Ion/Metal Batteries, Advanced Materials 34 (2022) 2107899. https://doi.org/10.1002/adma.202107899

[11] A. Gupta, A. Manthiram, Designing advanced lithium-based batteries for low-temperature Conditions, Advanced energy materials 10 (2020) 2001972. https://doi.org/10.1002/aenm.202001972

[12] Z. Wang, Z. Tong, Q. Ye, H. Hu, X. Nie, C. Yan, W. Shang, C. Song, J. Wu, J. Wang, Dynamic tuning of optical absorbers for accelerated solar-thermal energy storage, Nature communications 8 (2017) 1478. https://doi.org/10.1038/s41467-017-01618-w

[13] X. Li, G. Ni, T. Cooper, N. Xu, J. Li, L. Zhou, X. Hu, B. Zhu, P. Yao, J. Zhu, Measuring conversion efficiency of solar vapor generation, Joule 3 (2019) 1798-1803. https://doi.org/10.1016/j.joule.2019.06.009

[14] F. Yi, H. Ren, K. Dai, X. Wang, Y. Han, K. Wang, K. Li, B. Guan, J. Wang, M. Tang, Solar thermal-driven capacitance enhancement of supercapacitors, Energy & Environmental Science 11 (2018) 2016-2024. https://doi.org/10.1039/C8EE01244J

[15] Y. Lu, J. Guo, Z. He, Z. Gao, Y.-Y. Song, Direct access to NiCo-LDH nanosheets by electrochemical-scanning-mediated hydrolysis for photothermally enhanced energy storage capacity, Energy Storage Materials 48 (2022) 487-496. https://doi.org/10.1016/j.ensm.2022.03.050

[16] P. Ma, Y. Sun, X. Zhang, J. Chen, B. Yang, Q. Zhang, X. Gao, X. Yan, Spinel-type solar-thermal conversion coatings on supercapacitors: An effective strategy for capacitance recovery at low temperatures, Energy Storage Materials 23 (2019) 159-167. https://doi.org/10.1016/j.ensm.2019.05.016

[17] Y. Lu, J. Xu, C. Zhao, Z. Gao, Y.-Y. Song, Boosting the local temperature of hybrid Prussian blue/NiO nanotubes by solar light: effect on energy storage, ACS Sustainable Chemistry & Engineering 9 (2021) 11837-11846. https://doi.org/10.1021/acssuschemeng.1c03483

[18] T.G. Mayerhöfer, S. Pahlow, J. Popp, The Bouguer-Beer-Lambert law: Shining light on the obscure, ChemPhysChem 21 (2020) 2029-2046. https://doi.org/10.1002/cphc.202000464

[19] D.F. Swinehart, The beer-lambert law, Journal of chemical education 39 (1962) 333. https://doi.org/10.1021/ed039p333

[20] D.E. McCoy, T. Feo, T.A. Harvey, R.O. Prum, Structural absorption by barbule microstructures of super black bird of paradise feathers, Nature communications 9 (2018) 1. https://doi.org/10.1038/s41467-017-02088-w

[21] Z. Han, S. Niu, L. Zhang, Z. Liu, L. Ren, Light trapping effect in wing scales of butterfly Papilio peranthus and its simulations, Journal of Bionic Engineering 10 (2013) 162-169. https://doi.org/10.1016/S1672-6529(13)60211-5

[22] Z. Xie, H. Wang, M. Li, Y. Tian, Q. Deng, R. Chen, X. Zhu, Q. Liao, Photothermal trap with multi-scale micro-nano hierarchical structure enhances light absorption and promote photothermal anti-icing/deicing, Chemical Engineering Journal 435 (2022) 135025. https://doi.org/10.1016/j.cej.2022.135025

[23] H. Tao, J. Lin, Z. Hao, X. Gao, X. Song, C. Sun, X. Tan, Formation of strong light-trapping nano-and microscale structures on a spherical metal surface by femtosecond laser filament, Applied Physics Letters 100 (2012). https://doi.org/10.1063/1.4719108

[24] N.T. Panagiotopoulos, E.K. Diamanti, L.E. Koutsokeras, M. Baikousi, E. Kordatos, T.E. Matikas, D. Gournis, P. Patsalas, Nanocomposite catalysts producing durable, super-black carbon nanotube systems: applications in solar thermal harvesting, ACS nano 6 (2012) 10475-10485. https://doi.org/10.1021/nn304531k

[25] Q. Zhao, T. Fan, J. Ding, D. Zhang, Q. Guo, M. Kamada, Super black and ultrathin amorphous carbon film inspired by anti-reflection architecture in butterfly wing, Carbon 49 (2011) 877-883. https://doi.org/10.1016/j.carbon.2010.10.048

[26] M. Spinner, A. Kovalev, S.N. Gorb, G. Westhoff, Snake velvet black: hierarchical micro-and nanostructure enhances dark colouration in Bitis rhinoceros, Scientific reports 3 (2013) 1846. https://doi.org/10.1038/srep01846

[27] P. Tao, W. Shang, C. Song, Q. Shen, F. Zhang, Z. Luo, N. Yi, D. Zhang, T. Deng, Bioinspired engineering of thermal materials, Advanced Materials 27 (2015) 428-463. https://doi.org/10.1002/adma.201401449

[28] Q. Zhao, X. Guo, T. Fan, J. Ding, D. Zhang, Q. Guo, Art of blackness in butterfly wings as natural solar collector, Soft Matter 7 (2011) 11433-11439. https://doi.org/10.1039/C1SM06167D

[29] Q. Zhu, J. Yan, A mixed interface-capturing/interface-tracking formulation for thermal multi-phase flows with emphasis on metal additive manufacturing processes, Computer Methods in Applied Mechanics and Engineering 383 (2021) 113910. https://doi.org/10.1016/j.cma.2021.113910

[30] B. Liu, G. Fang, L. Lei, W. Liu, A new ray tracing heat source model for mesoscale CFD simulation of selective laser melting (SLM), Applied Mathematical Modelling 79 (2020) 506-520. https://doi.org/10.1016/j.apm.2019.10.049

[31] Q. Zhao, J. Wang, X. Ai, Z. Pan, F. Xu, J. Wang, Y. Gao, Large-area multifunctional electro-chromic-chemical device made of $W_{17}O_{47}$ nanowires by Zn^{2+} ion intercalation, Nano Energy 89 (2021) 106356. https://doi.org/10.1016/j.nanoen.2021.106356

[32] W. Wei, Y. Yao, Q. Zhao, Z. Xu, Q. Wang, Z. Zhang, Y. Gao, Oxygen defect-induced localized surface plasmon resonance at the WO_{3-x} quantum dot/silver nanowire interface: SERS and photocatalysis, Nanoscale 11 (2019) 5535-5547. https://doi.org/10.1016/j.apm.2019.10.049

[33] K. Li, T.H. Chang, Z. Li, H. Yang, F. Fu, T. Li, J.S. Ho, P.Y. Chen, Biomimetic MXene textures with enhanced light-to-heat conversion for solar steam generation and wearable thermal management, Advanced Energy Materials 9 (2019) 1901687. https://doi.org/10.1002/aenm.201901687

[34] J. Pang, L. Tao, X. Lu, Q. Yang, V. Pachauri, Z. Wang, S. Ingebrandt, X. Chen, Photothermal effects induced by surface plasmon resonance at graphene/gold nanointerfaces: A multiscale modeling study, Biosensors and Bioelectronics 126 (2019) 470-477. https://doi.org/10.1016/j.bios.2018.11.007

[35] X. Zhang, S. Lin, F. Zhao, J. Zhang, S. Lei, F. Bai, Q. Liu, J. Wu, T. He, P. Huang, Programmably Controllable Delivery of Metastable Ferrous Ions for Multiscale Dynamic Imaging Guided Photothermal Primed Chemodynamic Therapy, Advanced Materials (2023) 2210876. https://doi.org/10.1002/adma.202210876

[36] Z. Huang, C. Cao, Q. Wang, H. Zhang, C.E. Owens, A.J. Hart, K. Cui, Multiscale Plasmonic Refractory Nanocomposites for High-Temperature Solar Photothermal Conversion, Nano Letters 22 (2022) 8526-8533. https://doi.org/10.1021/acs.nanolett.2c03003

[37] C. Wang, X. Zhang, S. Liu, H. Zhang, Q. Wang, C. Zhang, J. Gao, L. Liang, H. Cao, Interfacial charge transfer and zinc ion intercalation and deintercalation dynamics in flexible multicolor electrochromic energy storage devices, ACS Applied Energy Materials 5 (2021) 88-97. https://doi.org/10.1021/acsaem.1c02508

[38] Z. Song, B. Wang, W. Zhang, Q. Zhu, A.Y. Elezzabi, L. Liu, W.W. Yu, H. Li, Fast and Stable Zinc Anode-Based Electrochromic Displays Enabled by Bimetallically Doped Vanadate and Aqueous Zn2+/Na+ Hybrid Electrolytes, Nano-Micro Letters 15 (2023) 229. https://doi.org/10.1007/s40820-023-01209-z

[39] R. Ren, S. Liu, Y. Gao, P. Lei, J. Wang, X. Tong, P. Zhang, Z. Wang, G. Cai, Tunable Interaction between Zn2+ and Superstructured Nb18W16O93 Bimetallic Oxide for Multistep Tinted Electrochromic Device, ACS Energy Letters 8 (2023) 2300-2307. https://doi.org/10.1021/acsenergylett.3c00484

[40] X. Ju, F. Yang, X. Zhu, X. Jia, Zinc ion intercalation/deintercalation of metal

organic framework-derived nanostructured NiO@ C for low-transmittance and high-performance electrochromism, ACS Sustainable Chemistry & Engineering 8 (2020) 12222-12229. https://doi.org/10.1021/acssuschemeng.0c03837

[41] J.-L. Wang, Y.-R. Lu, H.-H. Li, J.-W. Liu, S.-H. Yu, Large area co-assembly of nanowires for flexible transparent smart windows, Journal of the American Chemical Society 139 (2017) 9921-9926. https://doi.org/10.1021/jacs.7b03227

[42] J. Zhang, J.-p. Tu, X.-h. Xia, X.-l. Wang, C.-d. Gu, Hydrothermally synthesized WO_3 nanowire arrays with highly improved electrochromic performance, Journal of Materials Chemistry 21 (2011) 5492-5498. https://doi.org/10.1039/C0JM04361C

[43] Y. Tian, W. Zhang, S. Cong, Y. Zheng, F. Geng, Z. Zhao, Unconventional aluminum ion intercalation/deintercalation for fast switching and highly stable electrochromism, Advanced Functional Materials 25 (2015) 5833-5839. https://doi.org/10.1002/adfm.201502638

[44] Y. Ding, H. Sun, Z. Li, C. Jia, X. Ding, C. Li, J.-G. Wang, Z. Li, Galvanic-driven deposition of large-area Prussian blue films for flexible battery-type electrochromic devices, Journal of Materials Chemistry A 11 (2023) 2868-2875. https://doi.org/10.1039/D2TA08023K

[45] C. Wu, H. Shi, L. Zhao, X. Chen, X. Zhang, C. Zhang, J. Yu, Y. Lv, R. Wei, T. Gao, High-Performance Aqueous Zn^{2+}/Al^{3+} Electrochromic Batteries based on Niobium Tungsten Oxides, Advanced Functional Materials (2023) 2214886. https://doi.org/10.1002/adfm.202214886

[46] S. Cao, S. Zhang, T. Zhang, Q. Yao, J.Y. Lee, A visible light-near-infrared dual-band smart window with internal energy storage, Joule 3 (2019) 1152-1162. https://doi.org/10.1016/j.joule.2018.12.010

[47] Q. Zhao, J. Wang, Y. Cui, X. Ai, Z. Chen, C. Cao, F. Xu, Y. Gao, The discovery of conductive ionic bonds in NiO/Ni transparent counter electrodes for electrochromic smart windows with an ultra-long cycling life, Materials Advances 2 (2021) 4667-4676. https://doi.org/10.1039/D1MA00384D

[48] P. González-Borrero, F. Sato, A. Medina, M.L. Baesso, A.C. Bento, G. Baldissera, C. Persson, G.A. Niklasson, C.G. Granqvist, A. Ferreira da Silva, Optical band-gap determination of nanostructured WO_3 film, Applied Physics Letters 96 (2010). https://doi.org/10.1063/1.3313945

Highlights

- Solar-thermal conversion, as a novel and cost-effective method, was proposed to mitigate undesirable electrochromic performance in low-temperature conditions.

- Inspired by the super black feathers of the *Paradisaeidae*, a multiscale hierarchical structure was purposely designed to enhance the solar-thermal conversion.

- A high absorption of 87 % over the entire solar spectrum was achieved, along with rapid recovery of electrochromic performance at -20°C within merely 8 mins.

- The absorption mechanism and optical path were thoroughly elucidated using ray-tracing simulations.